Journal of The Electrochemical Society, 2022 **169** 034507
1945-7111/2022/169(3)/034507/12/$40.00 © 2022 The Electrochemical Society ("ECS"). Published on behalf of ECS by IOP Publishing Limited

Modeling of PEMFC and Analysis of Multiple Influencing Factors on Output Characteristics

Yang Yang,[1,2] Wen-Chao Zhu,[1] Yang Li,[1] Bo Zhao,[3] Lei-Qi Zhang,[3] Jie Song,[4] Zhan-Feng Deng,[4] Ying Shi,[2] and Chang-Jun Xie[1,2,z]

[1]*Hubei Key Laboratory of Advanced Technology for Automotive Components, Wuhan University of Technology, Wuhan 430070, People's Republic of China*
[2]*School of Automation, Wuhan University of Technology, Wuhan 430070, People's Republic of China*
[3]*State Grid Zhejiang Electric Power Research Institute, Hangzhou 310014, People's Republic of China*
[4]*Global Energy Interconnection Research Institute, Beijing 102211, People's Republic of China*

The output characteristics of the Proton-Exchange Membrane Fuel Cells (PEMFCs) are affected by multiple factors, but quantitatively describing the relationships is challenging. In this paper, a semi-empirical dynamic model of PEMFC is established firstly. The influence of a single factor on the output characteristics of PEMFC is analyzed longitudinally. Then, a derivative significance weight analysis based on support vector regression (SVR-DSWA) algorithm is proposed to analyze the influence weights of multi-factors on the output characteristics, and the optimal parameters combinations in different current density regions are obtained by maximizing the output voltage values based on formulated SVR model. The Root-Mean-Square Error (RMSE) of output voltage prediction results based on the SVR algorithm is less than 0.0458, and the accuracy of weight analysis results by using the SVR-DSWA algorithm and the optimal parameters combinations analysis method are verified by 4-factor 3-level orthogonal experiments in low, medium, and high current density regions. The SVR-DSWA algorithm and optimal parameters combinations analysis method can replace the orthogonal experiment to analyze the influence weights and optimal combinations of input factors on the output characteristics within the full current density range rapidly, and has much higher efficiency than the orthogonal experiment. The analysis results can provide theoretical support for improving fuel cell performance and formulating a control strategy.
 [DOI: 10.1149/1945-7111/ac580a]

Manuscript received December 8, 2021. Published March 4, 2022.

Due to its merits of large reserves and environmentally-friendly nature, hydrogen is considered a promising solution for developing future energy storage.[1] As a key power generation component of the hydrogen-based energy storage systems, a fuel cell can convert the chemical energy in the hydrogen into electricity and heat in a pollution-free and zero-emission manner.[2] Among various fuel cell technologies, the Proton-Exchange Membrane Fuel Cell (PEMFC) possesses distinct advantages: high energy and power densities, fast response, no electrolyte leakage and corrosion, and a favorable temperature range for practical applications.[3] An accurate mathematical model of the PEMFC is essential for verifying and predicting the effectiveness of new materials, innovative structural designs, and advanced system control strategies under different operating conditions. However, accurately and efficiently describing the complex dynamic behaviors of PEMFC, using multi-physical domain knowledge ranging from electrochemistry, hydrodynamics, and thermodynamics, are fundamentally challenging. Usually, a model should be developed to consider the research objectives and the applications. Different types of PEMFC models have different applicability to related problems. Accordingly, to predict the output performance of the PEMFC, the PEMFC models can be generally categorized into four types: (1) the mechanistic models, (2) the empirical models, (3) the semi-empirical models, and (4) the data-driven models. The advantages, disadvantages, and applications of these models are summarized in Table I.

When the working process to be studied needs for analyzing the internal mechanism characteristics of PEMFC, structural optimization, and material development, the corresponding *mechanism model* should be established. For example, Fuller et al.[4] first established a one-dimensional (1D) isothermal model for a small single cell. Nalbant et al.[5] showed a 1D steady-state model supplied by a mixture of hydrogen and carbon monoxide, where the effects of temperature, platinum loading, and the membrane materials on the performance of high-temperature PEMFC were studied. Rahman et al.[6] developed a 1D non-isothermal model to predict the resistance to dry oxygen and limiting current. Abdollahzadeh et al.[7] proposed a cathode two-dimensional (2D) multi-component mixture model to study the effects of pressure difference, operating temperature, Gas Diffusion Layer (GDL) thickness, GDL porosity, and inlet gas humidity on PEMFC performance. The 2D model considers the influence of changes, in the reaction gas transport along the flow channel, on the PEMFC performance.[8] Dutta et al.[9] used the three-dimensional (3D) model to predict the temperature behavior in the PEMFC channel for the first time. They studied the influence of heat generated by chemical reactions on the performance of the PEMFC. Kahveci et al.[10] established a 3D single-phase model to investigate the performance of PEMFC with winding channels, and analyzed the effects of operating pressure and temperature on the output performance. Although such a 3D model is a multi-domain coupling model that can accurately describe the transmission mechanism of PEMFC in the whole space,[9–11] the model structure is complex to derive, and many model parameters are difficult to obtain. In addition, the computational burden to solve these 3D models is prohibitive, which impedes the use of these models for practical control systems of PEMFCs.

The *empirical models* are established based on the empirical equations or equivalent circuits, and relevant model parameters are identified with experimental data of different types of PEMFCs.[12,13] An empirical model has a small set of parameters, simple model structures, and low computational costs and is mainly used in designing system control strategies and real-time simulation. However, the accuracy of the empirical models is low and not suitable for optimizing the system performance. In contrast, a *semi-empirical model* uses some knowledge of the PEMFC mechanisms to develop simple empirical equations instead of complex mechanistic equations. Some parameters that are difficult to determine can be obtained by parameter identification, which can be regarded as a simplification of the full-order mechanism models. The semi-empirical models can be used when the internal mechanisms of a PEMFC are difficult to describe accurately, or the details of the internal processes are insignificant to the applications. The semi-empirical models are suitable for structural optimization and system control. For instance, Corrêa et al.[14] proposed a semi-empirical dynamic electrochemical model as a function of the load current and several constructive and operational parameters to predict the output

[z]E-mail: jackxie@whut.edu.cn

Table I. Comparison of PEMFC modeling methods.

Modeling methods	Advantages	Disadvantages	Applications
Mechanism modeling	Describing internal mechanisms Accurate and detailed	Complex Difficult to solve High calculation cost	Characteristic analysis Structure optimization Material development
Semi-empirical modeling	Describing internal mechanisms Partial simplification of the model	Mechanism description is incomplete	Structure optimization System control
Empirical modeling	Simple equation Fewer parameters to calculate	Lack of internal mechanism description	Parameter optimization System control
Data-driven modeling	Not limited by physical parameters	Large data sets are required	Characteristics prediction

voltage, efficiency, and power of PEMFCs. Tirnovan et al.[15] measured voltage and current density under certain experimental conditions, established a numerical model, and analyzed the influence of operating pressures and temperatures on the cell voltage. Youssef et al.[16] developed a lumped model for PEMFC based on linear algebra equations, and studied the effects of several operating and design parameters on the performance of the fuel cells. These parameters include temperature, pressure, stoichiometric ratio, membrane thickness, and gas diffusion layer thickness. Tiss et al.[17] developed a nonlinear state-space model for describing a non-isothermal PEMFC, studied the effects of load resistance, hydrogen partial pressure, oxygen partial pressure, and liquid water in the gas diffusion layer on the dynamic performance of the fell. Nascimento et al.[18] and Lan et al.[19] developed equivalent circuit models considering electrothermal characteristics, studied the output characteristic curves and the transient response to load current and stack temperature change. Hernández-Gómez et al.[20] considered the influence of the current ripple of power electronic devices on cell performance, proposed a cell voltage static-dynamic model with adaptive parameters to consider the influence of the input current.

Due to the advancements of artificial intelligence, the rapidly increased computational capability of microprocessors, and the availability of big data, *data-driven models* are received extensive research attention in recent years. In such a method, a "black box" model is trained using a large number of experimental data, and the process does not need to involve the knowledge of internal mechanisms of the PEMFCs. Such a model can predict the behaviors with unknown mechanisms or when some physical parameters are difficult to obtain, but it requires a substantial high-fidelity dataset.[21,22] For example, Nanadegani et al.[23] developed a data-driven PEMFC voltage model using an artificial neural network, where the inputs of the model are temperature, excess coefficient of the anode and cathode gas, relative humidity, and load current. Wang et al.[24] proposed a surrogate modeling method that combines a state-of-the-art 3D PEMFC physical model and data-driven model, and established a multi-physics-resolved digital twin of PEMFCs, exhibited low requirements on computation.

The above studies have actively contributed to the longitudinal or local analyses of the impact of a single factor on the output performance of PEMFC but neglected the dependent effects of different factors. However, for a practical PEMFC system, the output characteristics of PEMFC are simultaneously affected by factors of water, heat, electricity, gas, force, amongst others. Therefore, it is beneficial to analyze the influence of multiple factors globally on the output characteristics of PEMFC. A multi-dimensional analysis can be used to obtain a more accurate description of how different factors can impact the output performance of PEMFC, and several recent studies show that the orthogonal experimental method is effective for relevant investigation.[25] Orthogonal experimental is a multi-factor and multi-level design method, according to orthogonality, representative points of "uniform dispersion" are selected from the comprehensive test for experiment. For example, Xia et al.[26] designed nine orthogonal experiments to study the effects of fuel cell operating temperature, inlet pressure, relative humidity, and oxidant stoichiometry on the performance of PEMFC. As a result, the optimal combination of operating parameters under different load current densities was found. Wang et al.[27] obtained the optimum levels of relative humidity, working temperature, and stoichiometric ratio of air by an orthogonal test.

However, the orthogonal experimental can only analyze the influence of multiple factors under a specific current density at a time. Multiple tests are required and more time consuming, when it is necessary to analyze the influence of multiple factors in the full current density region. Efficient and rapid analysis is needed. Therefore, establishing voltage prediction model based on limited data samples is considered for rapid analysis of multiple influencing factors. Support Vector Machine (SVM) is a powerful tool for Gaussian regression estimation and is suitable for small sample training. Its generalization performance is not affected by the dimension of input data and can consider both the complexity and generalization ability under the condition of a limited sample size. The technique has been applied to modeling PEMFC, parameter identification, and power density model optimization.[26,28–30] In this paper, to determine the sensitivity of the network output to the variation of partial derivatives of characteristic variables in the model prediction process and to determine the weights of characteristic variables, a Derivative Significance Weight Analysis based on Support Vector Regression (SVR-DSWA) algorithm is proposed.

This paper aims at analyzing the influence weights of multiple factors on the output characteristics and the optimal parameter combinations regarding the multiple factors. The main contributions of this work are:

1. The establishment of a semi-empirical dynamic model of PEMFC, which considers the dynamic partial pressure of cathode and anode gases and a delay between the change in load current and the flow of fuel and oxidizer.
2. The quickly analysis of the influence weights of multiple factors on the output characteristics within the total current density range based on the proposed SVR-DSWA algorithm.
3. Optimal parameter combination analysis for maximum output voltage using a standard simplex method based on SVR model optimization.
4. The verification of the accuracy of weight analysis results using the SVR-DSWA algorithm and optimal combination analysis method by 4-factors 3-levels orthogonal experiments.

The structure of this paper is as follows: The output voltage model is introduced in the second part. The verification of the model and the single factor longitudinal simulation analysis are introduced in the third part. In the fourth part, the key idea of SVR-DSWA algorithm and its implementation are described. In the fifth part, the results of multi-factors weight analysis using SVR-DSWA algorithm and optimal parameter combination analysis are presented, and compared with the results of orthogonal experiment. In the last part, the thesis is summarized.

PEMFC Model

Operating principles of PEMFC.—PEMFC is a low-temperature fuel cell using a solid polymer film as the electrolyte. The schematic of a typical PEMFC is illustrated in Fig. 1a. The PEMFC consists of two electrodes and an electrolyte sandwiched in between. Hydrogen enters the anode side of the membrane electrode from the anode air inlet, passes through the gas diffusion layer to the surface of the catalyst layer, and forms protons (H^+) and electrons (e^-) through an oxidation reaction. The corresponding reaction equation is as follows.

$$\text{Anode: } H_2 \rightarrow 2H^+ + 2e^- \quad [1]$$

Protons pass through the proton-exchange membrane (PEM) to the cathode, and electrons move to the cathode through the external circuit to generate electric currents.[14] On the other side of the cell, oxygen enters the cathode side of the membrane electrode from the cathode air inlet, and it combines with electrons and hydrogen ions that have passed through the PEM to generate water and release heat. The electrochemical reaction that happens in the cathode is

$$\text{Cathode: } 2H^+ + \frac{1}{2}O_2 + 2e^- \rightarrow H_2O + \text{Heat} \quad [2]$$

The complete chemical reaction can be expressed by

$$H_2 + \frac{1}{2}O_2 \rightarrow H_2O \quad [3]$$

Output voltage model of PEMFC.—A semi-empirical model of PEMFC is first developed in this section. In this work, the output voltage of PEMFC is expressed as a function of cell current, cathode

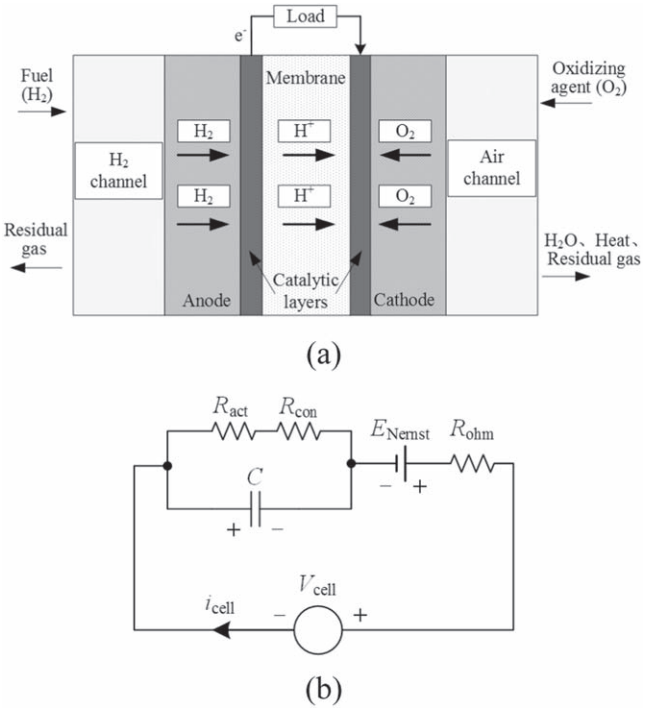

Figure 1. (a) Schematic of the PEMFC. (b) PEMFC equivalent circuit.

inlet pressure, anode inlet pressure, fuel cell temperature, and water content of the PEM. The stack voltage is calculated by scaling up the single-cell voltage with the number of connected cells in series.

In the steady-state, the output voltage of the PEMFC should be the thermodynamic electromotive force E_{Nernst}, i.e., the reversible electromotive force for an open circuit or the open-circuit voltage. During operations, various irreversible losses lead to the deviation of the cell voltage to E_{Nernst}, and these factors include the fuel and oxidant delays, activation polarization overvoltage (V_{act}), ohmic polarization overvoltage (V_{ohm}), and concentration polarization overvoltage (V_{con}).[31,32] In this condition, the output voltage can be expressed as

$$V_{\text{cell}} = E_{\text{Nernst}} - V_{\text{act}} - V_{\text{ohm}} - V_{\text{con}} \quad [4]$$

where the open-circuit voltage can be calculated by the Nernst equation,[14,32] i.e.,

$$E_{\text{Nernst}} = 1.229 - 8.5 \times 10^{-4} \times (T - 298.15) + \frac{RT}{2F} \ln\left[P^*_{\text{H}_2} \cdot (P^*_{\text{O}_2})^{0.5}\right] \quad [5]$$

In Eq. 5, R is the general gas constant, F is the Faraday constant, and T is the cell temperature. Furthermore, P_{H2} and P_{O2} are the effective partial pressures of hydrogen and oxygen, respectively, defined as[31,32]

$$P_{\text{H}_2} = 0.5RH^*_{\text{a}}P_{\text{H}_2\text{O}}\left[\left(\exp\left(\frac{1.635(i/A)}{T^{1.334}}\right) \times \frac{RH^*_{\text{a}}P_{\text{H}_2\text{O}}}{P_{\text{a}}}\right)^{-1} - 1\right] \quad [6]$$

$$P_{\text{O}_2} = RH^*_{\text{c}}P_{\text{H}_2\text{O}}\left[\left(\exp\left(\frac{4.192(i/A)}{T^{1.334}}\right) \times \frac{RH^*_{\text{c}}P_{\text{H}_2\text{O}}}{P_{\text{c}}}\right)^{-1} - 1\right] \quad [7]$$

where i is the load current and A is the activation area. P_{a} and P_{c} are the inlet gas pressures of anode and cathode, respectively. RH_{a} and RH_{c} are the relative humidity of water vapor of anode and cathode, respectively. P_{H2O} represents the saturated partial pressure of water vapor, which is calculated by [33,34]

$$\log 10(P_{\text{H}_2\text{O}}) = 2.95 \times 10^{-2}(T - 273.15) - 9.18 \times 10^{-5} \times (T - 273.15)^2 + 1.44 \times 10^{-7}(T - 273.15)^3 - 2.18 \quad [8]$$

During transient, a delay can be observed between the change in load current and the fuel and oxidizer flow. In order to simplify the analysis, the overall impact of the delay is considered by subtracting a term E_{d} from the right-hand side of Eq. 5. Here, E_{d} is given by [31]

$$E_{\text{d}} = \lambda_{\text{e}}[i - i \otimes \exp(-t/\tau_{\text{e}})] \quad [9]$$

where $\otimes$ represents the tensor product, τ_{e} is the total delay time of the flow of fuel and oxidant and λ_{e} is the gain. The revised open-circuit voltage is thus expressed as

$$E'_{\text{Nernst}} = E_{\text{Nernst}} - \lambda_{\text{e}}[i - i \otimes \exp(-t/\tau_{\text{e}})] \quad [10]$$

The activation overvoltage V_{act} is the potential barrier to be overcome when electrons move between the electrodes, as well as due to the destruction and recombination of chemical bonds in the chemical reaction between the anode and cathode.[30] The activation overvoltage includes the loss of cathode and anode activation, calculated as below:[14]

$$V_{\text{act}} = -(\varepsilon_1 + \varepsilon_2 T + \varepsilon_3 T \ln A + \varepsilon_4 T \ln C_{\text{H}_2} + \varepsilon_5 T \ln C_{\text{O}_2} + \varepsilon_6 T \ln i) \quad [11]$$

where $\varepsilon_1 - \varepsilon_6$ are fitting coefficients. C_{O2} and C_{H2} are the mass fractions of oxygen and hydrogen concentrations, respectively, and they can be obtained by Henry's law.[33]

$$C_{\text{O}_2} = \frac{P_{\text{O}_2}}{5.08 \times 10^6 \times \exp\left(\frac{-498}{T}\right)}, \quad C_{\text{H}_2} = \frac{P_{\text{H}_2}}{1.09 \times 10^6 \times \exp\left(\frac{77}{T}\right)} \quad [12]$$

The ohmic overvoltage V_{ohm} is the voltage drop on the resistance R_{c} when electrons move between the electrodes and the resistance R_{a} when protons pass through the membrane. The ohmic overvoltage can be expressed as[33,34]

$$V_{\text{ohm}} = i(R_{\text{a}} + R_{\text{c}}) = i\left(\frac{\rho_{\text{m}} \times l}{A} + R_{\text{c}}\right) \quad [13]$$

where l is the thickness of the PEM. The resistivity ρ_{m} can be calculated as

$$\rho_{\text{m}} = \frac{181.6 \times \left[1 + 0.03 \times \frac{i}{A} + 0.062 \times \left(\frac{T}{303}\right)^2 \times \left(\frac{i}{A}\right)^{2.5}\right]}{\left(\lambda - 0.634 - \frac{3i}{A}\right)\exp\left(4.18 \times \frac{T - 303}{T}\right)} \quad [14]$$

where λ is the water content of the PEM.

Next, the mass diffusion from the flow channel to the catalyst surface will form a concentration gradient.[34] The concentration loss is significant when the current density J is high, which is the leading cause of the voltage loss. The water film of catalyst on the surface of anode and cathode is another reason for the pressure drop. According to Fick's first law and Faraday's law, the concentration overvoltage V_{con} can be expressed by[33]

$$V_{con} = -\frac{RT}{2F}\ln\left(1 - \frac{J}{J_{max}}\right) + \frac{\varepsilon_7 \exp(\varepsilon_8 i - \varepsilon_9/P_c)}{P_c} \quad [15]$$

where J_{max} is the maximum current density, $\varepsilon_7 - \varepsilon_9$ are fitting coefficients.

As mentioned earlier, the PEM allows hydrogen ions to transport between the two electrodes and prevents electrons from passing through. Electrons flow from the anode through an external load and collect on the surface of the cathode, while hydrogen ions are attracted to the interface cathode membrane. The boundary between the porous electrode and the PEM forms two charged layers with opposite polarities, which causes the double-layer capacitance effect. The accumulation of the charges generates a voltage that combines the activation overvoltage and the concentration overvoltage. Due to the double-layer capacitance effect, when the load current varies, there is a lag in the change of the activation overvoltage and the concentration overvoltage, whereas it does not affect the ohmic voltage. An equivalent circuit in Fig. 1b can be used to simulate the double-layer capacitance effect, mathematically

$$V_C - V_0 = \left(i - C\frac{dV_C}{dt}\right)(R_{act} + R_{con}) \quad [16]$$

where C is the equivalent double-layer capacitance, V_C is the voltage at both ends of capacitor C, and V_0 is the voltage drop when under no-load conditions, expressed as[31]

$$V_0 = 0.279 - 8.5 \times 10^{-4}(T - 298.15) + 4.308 \times 10^{-5} \times T \times \left[\ln\left(\frac{P_c - P_{H_2O}}{1.01325}\right) + 0.5\ln\left(\frac{0.1173(P_c - P_{H_2O})}{1.01325}\right)\right] \quad [17]$$

By considering the double-layer capacitance, the cell voltage V_{cell} of PEMFC can be modified to

$$V_{cell} = E'_{Nernst} - V_C - V_{ohm} \quad [18]$$

Finally, the output voltage of the PEMFC stack with n cells can be calculated by

$$V_{stack} = nV_{cell} \quad [19]$$

Model verification and simulation analysis

Model verification.—In order to verify the proposed model, two different sets of parameters of PEMFC stacks are used in our work, and we refer them to as Stack 1 and Stack 2, respectively.

Table II shows the basic parameters of Stack 1, which are obtained from Refs. 34, 35, and the parameters of the output voltage model proposed in this paper. Three sets of experimental data from Ref. 33 are selected for model verification. Considering the operation range of the stack and the rationality of the model verification, $P_a/P_c/T$ corresponding to the three sets of experimental data are 3 bar/5 bar/353.15 K, 1 bar/1 bar/343.15 K, and 2.5 bar/3 bar/343.15 K, respectively. As shown in Fig. 2a, the RMSE between the simulation results and the experimental data is 0.519 V, and the Mean Relative Error (MRE) is 5.016%.

The parameters of Stack 2 are shown in Table III.[14,31] The parameters were obtained from an SR-12 Modular PEM Generator manufactured by Avista Laboratories. There are 37 sets of manufacturer data generated by the SR-12 Modular PEM Generator. This PEMFC is a modular fuel cell stack and has some characteristics adequate for use in electrical generation systems. The simulated voltage is shown in Fig. 2b, where it shows that the RMSE between the simulated voltage and the experimental data is 0.424 V, and the MRE is 1.11%. The results show that the accuracy of the proposed model is comparable and higher than the existing methods in Refs. 18, 19, e.g., the MRE described in the Ref. 18 is 1.26%.

The above results verify the static relationship based on the simulated *I-V* curves. Next, we use Stack 2 to further verify the model accuracy in terms of the dynamic response based on the parameters in Table III. Figure 3 shows the multiple-step responses of the proposed model when the load current changes rapidly, and the transients are validated by comparing the simulation results with the reference data of the 500-W SR-12 Avista Labs PEMFC reported in Refs. 18, 31. As shown in Fig. 3, when the load current rises from 5 A to 9 A at 210.35 s, the voltage drops to about 33 V due to the instantaneous change of ohmic overvoltage. Due to the double capacitance effect, the voltage gradually decreases to 32.5 V. Corresponding observations are made for the following fast step load changes. It can be observed that the fast transients are in close agreement with the experimental data.

Table II. Parameters of PEMFC Stack 1 and the proposed model.

Parameters	Value	Parameters	Value
n	24	ε_1	−0.9514
A (cm^2)	27	ε_2	0.00286
l (μm)	127	ε_3	0.0002
J_{max} ($A{\cdot}cm^{-2}$)	0.86	ε_4	4.3×10^{-5}
Rated Power (W)	250	ε_5	7.4×10^{-5}
P_a (bar)	1−3	ε_6	-1.87×10^{-4}
P_c (bar)	3−5	ε_7	3.8337×10^{-6}
T (K)	343.15−353.15	ε_8	0.467
RH_a	1	ε_9	0.1855
RH_c	1	Rc (Ω)	0.0001
R (J/(K·mol))	8.314	C (F)	2.5
F (C/mol)	96485	λ	23

Single-factor longitudinal simulation analysis.—The simulation parameters are set according to the parameters of the PEMFC stack, as shown in Table I. Figure 4a shows the output voltage and polarization overvoltage of a single cell changing with load current when the cell temperature is 70 °C, the inlet pressures of anode and cathode are 1 bar, and the water content of membrane is 23. As shown in Fig. 4a, the output voltage decreases with the increase of current due to the influence of irreversible electromotive force. The activation overvoltage increases with the increase of load current, but the increasing trend is slower and slower. The ohmic overvoltage rises almost linearly with the increase of load current. The concentration overvoltage rises with the increase of load current. In the low current density region, the concentration overvoltage slowly increases in a linear manner. In the high current density region, the concentration overvoltage rises sharply, and the trend is getting steeper and steeper.

Figures 4b–4e show the output voltage curves of the PEMFC stack when a single factor changes.

Figure 4b shows the PEMFC output voltage curves when the operating temperature is 343.15 K, 348.15 K, and 353.15 K, respectively, and P_a, P_c, and λ are 2.5 bar, 3 bar, and 23 bar, respectively. When the current is the same, the higher the working temperature is, the greater the output voltage is. Because the increase of temperature will increase catalyst activity, the water diffusion and gas diffusion ability in the membrane will be improved, which will reduce the membrane resistance and improve the output performance.

In Fig. 4c, T, P_c, and λ are 343.15 K, 3 bar, and 23, respectively. In Fig. 4d, T, P_a, and λ are 343.15 K, 2.5 bar, and 23, respectively. It can be seen from Figs. 4c and 4d that for the same current, higher anode and cathode pressures generally lead to better output performance of the cell. This is because increasing the inlet pressure of anode and cathode can increase the effective partial pressure of the hydrogen and oxygen, leading to an increase in the gas concentration and accelerating the chemical reaction.

Figure 4e shows the PEMFC output voltage curves when the water content of the membrane is 14, 18.5, and 23, respectively, and P_a, P_c, and T are 2.5 bar, 3 bar, and 343.15 K, respectively. Under the same current, increasing the membrane water content will increase the output voltage of the stack. The reason is that when

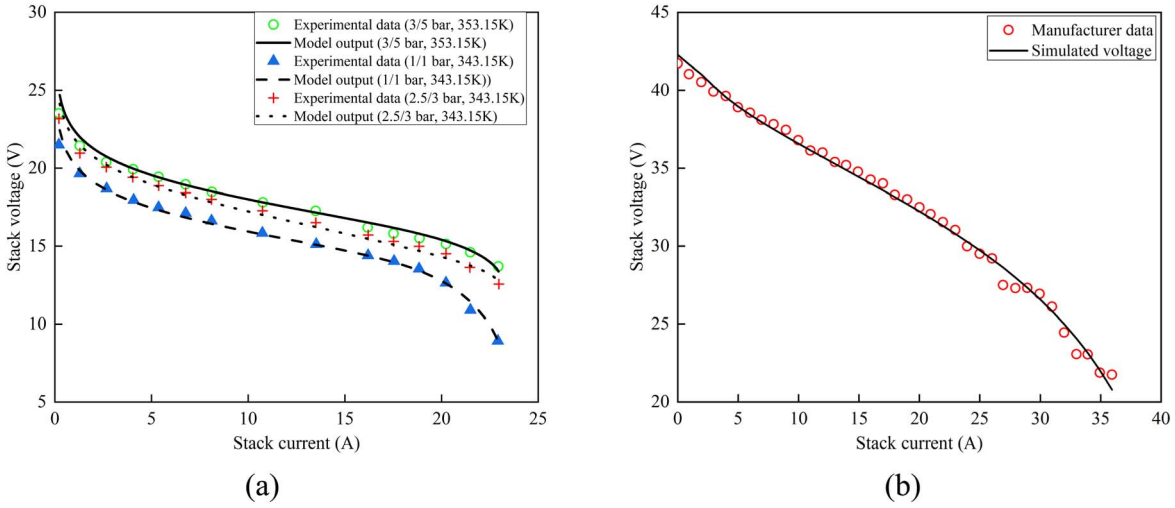

Figure 2. (a) The polarization curve of the PEMFC Stack 1. (b) The polarization curve of the PEMFC Stack 2.

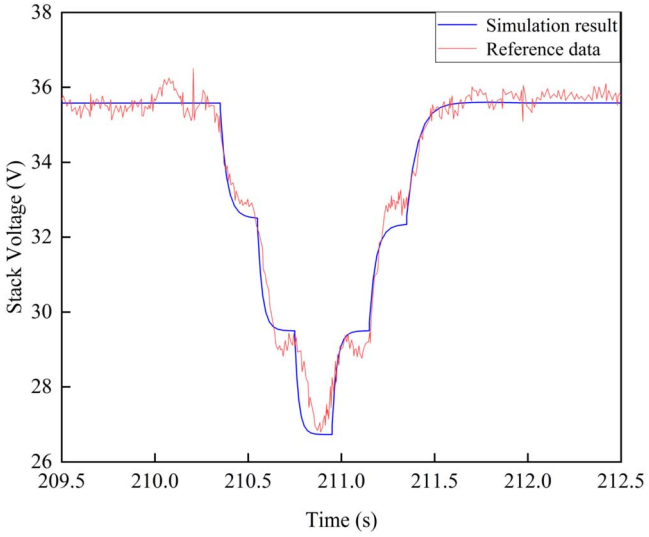

Figure 3. Transient response of the proposed model.

the membrane water content increases, the proton conduction velocity increases, and the membrane resistance decreases, which improves the output performance.

SVR- DSWA Algorithm

When an SVM is used for regression analysis, a nonlinear mapping $\Phi(x)$ is used to map the input vector to a high-dimensional feature space. Then, linear regression is carried out in the high-dimensional feature space to find the optimal hyperplane and minimize the error of all samples from the optimal hyperplane.[28]

Support vector regression.—The training sample set is $\{(x_i, y_i), i = 1, 2, \cdots, N\}$, N is the number of samples, x_i is the input value, and y_i is the expected output value. The regression model of the SVM is:

$$f(x) = w{\cdot}\Phi(x) + b \qquad [20]$$

where w and b are weight vector and bias, respectively.

The penalty factor c and relaxation variable ξ_i $(i = 1, 2, \cdots, N)$ are introduced under the insensitive loss function ε. Then, the solution of SVR becomes an optimization problem:

Table III. Parameters of the SR-12 modular PEM Generator and the proposed model.

Parameter	Value	Parameter	Value
n	48	ε_1	−0.9514
A (cm^2)	62.5	ε_2	0.00286
l (μm)	25	ε_3	0.0002
J_{max} (A/cm^{-2})	0.672	ε_4	4.3×10^{-5}
Capacity (W)	500	ε_5	7.4×10^{-5}
λ_e (Ω)	0.00333	ε_6	-1.87×10^{-4}
τ_e (s)	80	ε_7	3.8337×10^{-6}
T (K)	323.15	ε_8	0.467
P_{H2} (atm)	1.47628	ε_9	0.1855
P_{O2} (atm)	0.2095	λ	23
P_c (atm)	≈1	C (F)	1
R (J/(K·mol))	8.314	R_c (Ω)	0.0003
F (C mol^{-1})	96485		

$$\begin{cases} \min\limits_{w,b} \dfrac{1}{2}\|w\|^2 + c\sum\limits_{i=1}^{N}(\xi_i + \xi_i^*) \\ \text{s.t.} \begin{cases} y_i - w{\cdot}\Phi(x) - b \leqslant \varepsilon + \xi_i \\ y_i - w{\cdot}\Phi(x) - b \geqslant -\varepsilon - \xi_i^* \end{cases} \\ \xi_i, \xi_i^* \geqslant 0, (i = 1, 2, \cdots, N) \end{cases} \qquad [21]$$

By introducing Lagrangian multiplier $\{\alpha_i, \alpha_i^*, \beta_i, \beta_i^*, (i = 1, 2, \cdots, N)\}$, Eq. 21 can be rewritten as follows:

$$\begin{aligned} \min_{w,b} L(w, b, \xi, \xi^*) = {} & \frac{1}{2}\|w\|^2 + c\sum_{i=1}^{N}(\xi_i + \xi_i^*) \\ & - \sum_{i=1}^{N}\alpha_i[\varepsilon + \xi_i - y_i + w{\cdot}\Phi(x_i) + b] \\ & - \sum_{i=1}^{N}\alpha_i^*[\varepsilon + \xi_i^* + y_i - w{\cdot}\Phi(x_i) - b] \\ & - \sum_{i=1}^{N}(\beta_i\xi_i + \beta_i^*\xi_i^*) \end{aligned} \qquad [22]$$

Taking the partial derivative of w, b, ξ_i, and ξ_i^* in Eq. 22, we can get:

$$\begin{cases} \dfrac{\partial L}{\partial w} = w - \sum_{i=1}^{N} (\alpha_i - \alpha_i^*)\cdot\Phi(x_i) = 0 \\ \dfrac{\partial L}{\partial b} = -\sum_{i=1}^{N} (\alpha_i - \alpha_i^*) = 0 \\ \dfrac{\partial L}{\partial \xi_i} = c - \alpha_i - \beta_i = 0 \\ \dfrac{\partial L}{\partial \xi_i^*} = c - \alpha_i^* - \beta_i^* = 0 \end{cases} \quad [23]$$

Substituting Eq. 23 into Eq. 22, the dual form of Eq. 21 can be obtained:

$$\begin{aligned} &\max_{\alpha,\alpha^*} \sum_{i=1}^{N} (\alpha_i - \alpha_i^*) y_i - \sum_{i=1}^{N} (\alpha_i + \alpha_i^*)\varepsilon \\ &-\frac{1}{2}\sum_{i=1}^{N}\sum_{j=1}^{N} (\alpha_i - \alpha_i^*)(\alpha_j - \alpha_j^*)\Phi(x_i)\Phi(x_j) \\ &\text{s.t.} \sum_{i=1}^{N} (\alpha_i - \alpha_i^*) = 0 \\ &\alpha_i \geqslant 0,\ \alpha_i^* \leqslant c,\ (i = 1, 2, \cdots, N) \end{aligned} \quad [24]$$

Introduce the kernel function $K(x_i, x_j) = \Phi(x_i)\Phi(x_j)$ to map the data from the low-dimensional space to the high-dimensional space, thereby transforming the linearly inseparable problem into a linearly separable problem and converting the inner product calculation of the high-dimensional space to the function calculation of the low-dimensional space. According to the quadratic programming method, the optimal solution (α_i, α_i^*) of Eq. 24 is obtained, and the decision function of SVR is obtained as:

$$f(x) = \sum_{i=1}^{N} (\alpha_i - \alpha_i^*) K(x_i, x_j) + b \quad [25]$$

Since the Radial Basis Function (RBF) has the advantages of high accuracy and low computational complexity, RBF is used for training and prediction, which is defined as:

$$K(x_i, x_j) = \exp(-\gamma \|x_i - x_j\|^2) \quad [26]$$

where γ is the undetermined nuclear parameter.

The prediction results are evaluated by MRE, Mean Absolute Error (MAE), Mean Square Error (MSE), RMSE, and Squared Correlation Coefficient (R^2).

Derivative significance weight analysis.—The derivative significance analysis method based on SVR can be used to analyze the influence weight of input value on the expected output value.

It can be seen from Eq. 25 that only training samples corresponding to non-zero coefficients ($\alpha_i - \alpha_i^*$) can be used by decision functions. Therefore, the decision function can be expressed as:

$$f(x_i) = \sum_{j=1}^{N_S} (a_j - a_j^*) K(x_i, x_j) + b \quad [27]$$

where N_s is the number of support vectors.

The sensitivity of SVR network output to the kth characteristic input can be approximately obtained by calculating the partial derivative.

$$\begin{aligned} \frac{\partial f(x_i)}{\partial x_{ik}} &= \frac{\partial\left(\sum_{j=1}^{N_S} (\alpha_j - \alpha_j^*) K(x_i, x_j) + b\right)}{\partial x_{ik}} \\ &= \frac{\partial \sum_{j=1}^{N_S} (\alpha_j - \alpha_j^*) K(x_i, x_j)}{\partial x_{ik}} + \frac{\partial b}{\partial x_{ik}} \\ &= \sum_{j=1}^{N_S} (\alpha_j - \alpha_j^*) \frac{\partial K(x_i, x_j)}{\partial x_{ik}} = \\ &-2\gamma \sum_{j=1}^{N_S} (\alpha_j - \alpha_j^*)\cdot(x_{ik} - x_{jk}) \exp\left[-\gamma \sum_{l=1}^{K} x_{il} - x_{jl}^{\ 2}\right] \end{aligned} \quad [28]$$

In Eq. 28, K is the number of feature input quantities. The significance coefficient of the kth feature input is calculated as the sensitivity absolute average of the output value of all training data in the training set $\{(x_i, y_i), i = 1, 2, \cdots, N\}$ to the input value. The value can be expressed as:

$$S(k) = \frac{\sum_{i=1}^{N} \left| \frac{\partial f(x_i)}{\partial x_{ik}} \right|}{N} \quad [29]$$

The influence weight of the kth feature input on the prediction result $f(x)$ is:

$$C(k) = \frac{S(k)}{\sum_{k=1}^{K} S(k)} \quad [30]$$

Substituting Eqs. 28 and 29 into Eq. 30 yields the weight of the kth feature input:

$$C(k) = \frac{\sum_{i=1}^{N} \left| -2\gamma \sum_{j=1}^{N_S} (a_j - a_j^*)(x_{ik} - x_{jk}) \exp\left[-\gamma \sum_{l=1}^{K} (x_{il} - x_{jl})^2\right] \right|}{\sum_{k=1}^{K}\sum_{i=1}^{N} \left| -2\gamma \sum_{j=1}^{N_S} (a_j - a_j^*)(x_{ik} - x_{jk}) \exp\left[-\gamma \sum_{l=1}^{K} (x_{il} - x_{jl})^2\right] \right|} \quad [31]$$

SVR-DSWA algorithm implementation.—The process of using MATLAB to implement the SVR-DSWA algorithm is shown in Fig. 5, which includes eight steps as follows.

Step 1: Construct training set and test set. According to the given n data samples, select N data samples as the training set. The remaining (n–N) data samples are used as the test set.

Step 2: Normalize the data sample. The mapminmax function is used to normalize the data samples to [−1, 1] to improve the convergence speed and accuracy of SVR.

Step 3: Parameter optimization. The Gaussian radial basis kernel function is used for training and prediction. The grid search method combined with the ten-fold cross-validation method is used to find the optimal penalty factor c and the kernel parameter γ. The training set is randomly divided into ten parts, nine of which are used as the training set, and one is used as the validation set. The training set and validation set are iterated alternately ten times. In each iteration, the prediction model is trained with the `svmtrain` function, and the RMSE e_i of the prediction model is recorded, and then the average

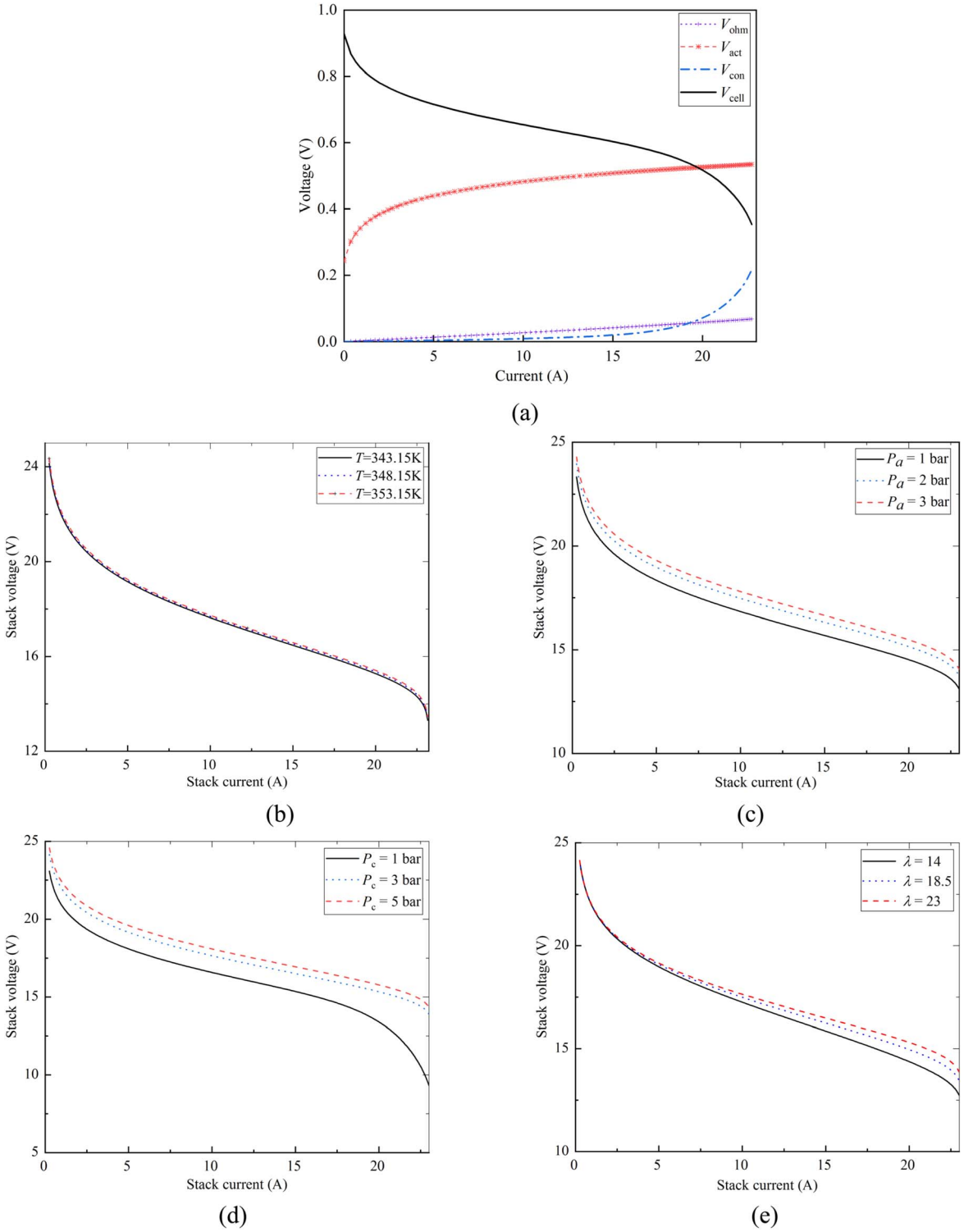

Figure 4. (a) voltage vs current curve of a single cell. (b) Stack voltages When T changes. (c) Stack voltages When P_a changes. (d) Stack voltages When P_c changes. (e) Stack voltages When the membrane water content changes.

value $E_1 = \frac{1}{10}\sum_{i=1}^{10} e_i$ is obtained. Next, change the parameters, traverse the grid to train the model for m rounds, and get the average RMSE E_m of each round of training. Obtain the minimum value of E_m, and determine the optimal parameters of the model.

Step 4: Find out the prediction result. The prediction model is trained with the optimal parameters, and the prediction model is used to predict (n–N) test samples to obtain the output value of the model.

Step 5: Analyze the forecast results. Denormalize the predicted output data and compare them with the experimental data. Calculate MRE, MAE, MSE, RMSE, and R^2 between the predicted value and the experimental data. Analyze the predicted results.

Step 6: Construct the training sample input matrix and support vector matrix. Find all training samples corresponding to non-zero coefficients ($\alpha_i - \alpha_i^*$), i.e., the support vectors. Construct training sample input matrix $\boldsymbol{X}_{N\times K}$ and support vector-matrix $\boldsymbol{V}_{Ns\times K}$, where N is the number of training samples, K is the number of

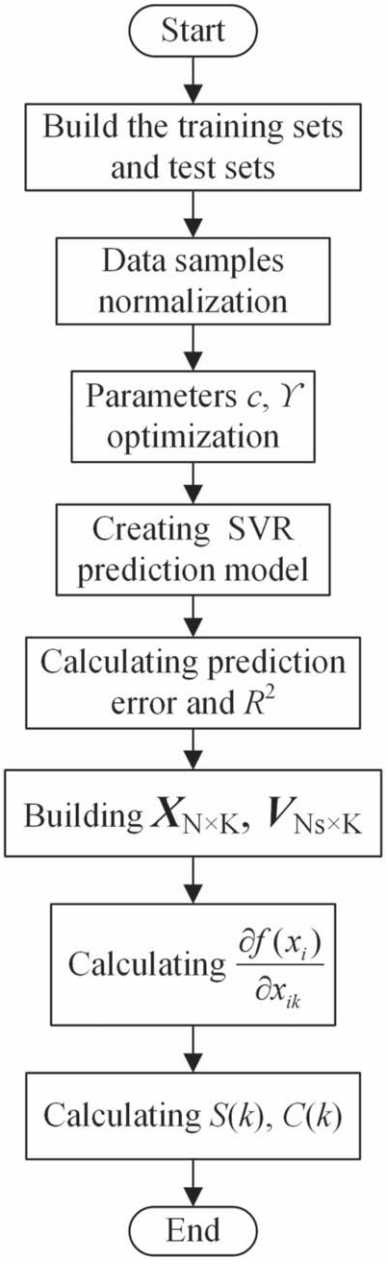

Figure 5. Flow chart of the SVR-DSWA algorithm.

influencing factors, N_s is the number of support vectors, and $N_s \leqslant N$.

Step 7: Calculate the partial derivative of the decision function. According to the optimal kernel parameter γ of the Gauss radial basis kernel function and the coefficient of the support vector $(\alpha_i - \alpha_i^*)$, the partial derivative $\partial f(x_i)/\partial x_{ik}$ of the decision function of the kth input variable is calculated.

Step 8: Calculate the significance coefficient and weight. According to the mean value of the absolute value of the partial derivative of the decision function of all training samples of the kth influencing factor, the corresponding significance coefficient $S(k)$ is calculated. Calculate the weight $C(k)$ of the kth influencing factor according to $S(k)$.

Results and Discussion

The numerical experiments are based on the PEMFC Stack 1 obtained from Refs. 33–35.

Prediction results.—The stack temperature affects the gas diffusion ability and proton conduction of the membrane. The inlet gas pressures of anode and cathode affect the chemical reaction rate. The cathode gas pressure also affects the discharge of water generated by the cathode reaction. When the PEM is flooded, the catalyst activity decreases, accelerating material corrosion and catalyst loss, resulting in a poor gas flow, which affects the performance and service life of the cell. When the membrane is dry, the proton conduction capacity decreases significantly, the membrane resistance increases, and the PEM will be burned in serious cases. Stack temperature, inlet gas pressure of cathode and anode and water content of PEM are the main factors affecting the performance of PEMFC, therefore, taking T, P_a, P_c, and λ as characteristic inputs, and PEMFC output voltage as output, an SVR-based PEMFC output performance prediction model is established. In the low, medium, and high current regions, the corresponding stack operating currents are set as 2 A, 12 A, and 22 A, respectively. The output voltage model proposed in this paper is used to simulate 150 sets of data samples. Among them, 120 sets of data are randomly selected as training samples, and the remaining 30 sets of data as test samples. Use the trained PEMFC output performance prediction model to predict the output voltage of the test sample, and the prediction results are shown in Figs. 6a–6c. It can be seen that the predicted results are in good agreement with the experimental data.

To verify the accuracy of the SVR-based PEMFC output performance model, the test samples are predicted every 1 A within the full current density range (operating current is 1 A–23 A). The errors and R^2 between the predicted result and the experimental data are shown in Figs. 6d. Figure 6d shows that the MRE between the predicted result and the experimental data is less than 0.51%, the MAE is less than 0.0657, the MSE is less than 0.0021, the RMSE is less than 0.0458, and R^2 is higher than 99.36% within the current range of 1 A–22 A, R^2 is higher than 97.78% within the current range of 22 A–23 A. The prediction accuracy of the SVR model is very high.

Weight and optimal levels analysis.—The SVR-DSWA algorithm is used to analyze the influence degrees of multiple factors on the output performance of the PEMFC. The standard simplex approach is used for performing the optimization of the formulated SVR model. The objective function is to maximize the output voltage, to obtain the optimal levels of different factors at a given current density.

In the low, medium, and high current density regions, respectively, a 4-factors 3-levels L_9 (3^4) orthogonal experiment is performed, 4-factors 3-levels are shown in Table IV. Then the accuracy of analysis results of the SVR-DSWA algorithm and the standard simplex approach are verified by comparing with orthogonal experiment results.

In the low, medium, and high current regions, when the operating current of the stack is 2 A, 12 A, and 22 A, the orthogonal experiment results and the SVR-DSWA algorithm analysis results are shown in Table V–VII, respectively. K_1, K_2, and K_3 respectively represent the average value of the output voltage of the stack obtained from three experiments for each factor. R is the range of the average value. The higher the R is, the greater the influence of the level change of this factor on the output voltage, and the greater the weight of the factor is. Table VIII shows optimal levels of different factors analyzed by the standard simplex approach and the influence degrees.

As shown in Table VIII, among the four factors, the factor that has the greatest influence on PEMFC output performance is cathode inlet gas pressure. The influence of operating temperature is minimal. At 2 A and 12 A, the order of the influence degree of the four factors on the output voltage is: R (C) > R (B) > R (D) > R (A) and P_c (C) > P_a (B) > λ (D) > T (A). At 22 A, the order of the influence degree of the four factors on the output voltage is: R (C) > R (D) > R (B) > R (A) and P_c (C) > λ (D) > P_a (B) > T (A). For

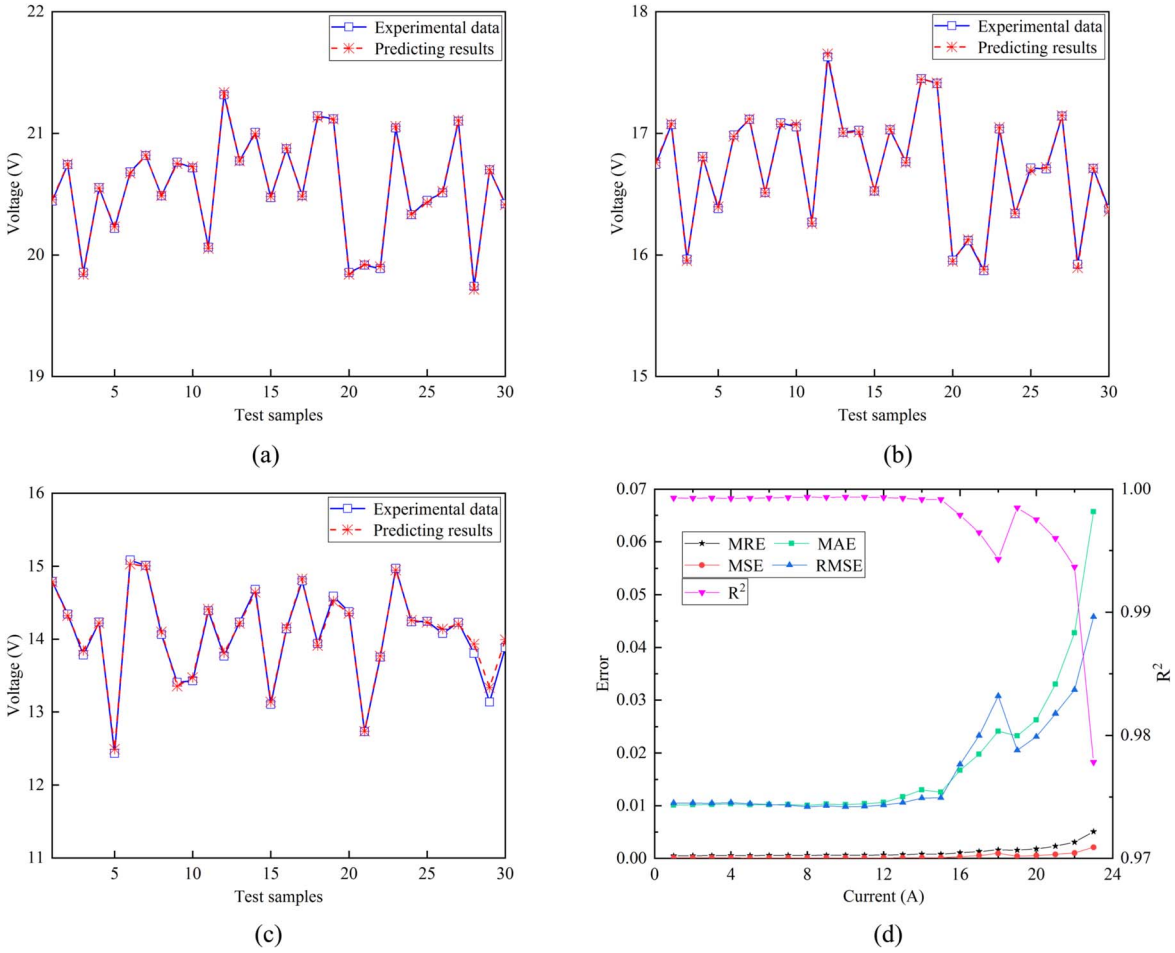

Figure 6. (a) Prediction results at 2 A. (b) Prediction results at 12 A. (c) Prediction results at 22 A. (d) Errors and R^2 between the prediction result and the experimental data.

Table IV. The combinations of operating parameters with 4-factors 3-levels.

Levels	A (T/K)	B (P_a/bar)	C (P_c/bar)	D (λ)
1	343.15	1	1	14
2	348.15	2	3	18.5
3	353.15	3	5	23

different levels of a certain factor, the maximum value of K_1, K_2, and K_3 determines the optimal level of this factor. At 2 A, the optimal levels of T, P_a, P_c, and λ are A2 (348.15 K), B3 (3 atm), C3 (5 atm), and D1 (14), respectively. At 12 A, the optimal levels of T, P_a, P_c, and λ are A2 (348.15 K), B3 (3 atm), C3 (5 atm), and D3 (23), respectively. At 22 A, the optimal levels of T, P_a, P_c, and λ are A3 (353.15 K), B3 (3 atm), C3 (5 atm), and D3 (23), respectively.

The analysis results of the SVR-DSWA algorithm and the standard simplex approach are consistent with the results of the orthogonal experiment, which proves their feasibility. However, using the orthogonal experiment method can only analyze the weight of influencing factors at a given current density each time, so the efficiency is low. The influence weights of the four factors on the output voltage in the full current density regions can be rapidly analyzed by using the SVR-DSWA algorithm. As shown in Fig. 7, when the current is in the range of 0–20 A, the order of influence degree is $P_c > P_a > \lambda > T$, and when the current is in the range of 20 A–23.22 A, the order of influence degree is $P_c > \lambda > P_a > T$. The cathode and anode inlet pressures have great influence on PEMFC output performance, which is in agreement with the analysis of Derbeli et al.[36] The temperature has little impact on output performance, and this conclusion agrees with the results obtained by Xia et al.[26] and Derbeli et al.[36] Furthermore, the influence of cathode inlet gas pressures is the largest within the full current density region, but the influence degree of anode inlet gas pressure decreases with the increase of current. The influence degree of operating temperature on the output voltage has little change with the increase of current. The influence degree of membrane water content on the output performance increases with the increase of current. Under the condition of low and medium current density, the effect of anode inlet gas pressure is larger than the effect of membrane water content. However, under the high current density, the effect of membrane water content is larger. The above conclusions are also consistent with the results of single-factor longitudinal simulation analysis, this further proves the reliability of the SVR-DSWA algorithm.

Conclusions

This paper establishes a semi-empirical dynamic output voltage model of PEMFC. An SVR-DSWA algorithm is proposed to analyze the influence weights of four factors (Operating temperature, inlet pressure of anode, inlet pressure of cathode, and water content of PEM) on the output characteristics of the PEMFC. The standard simplex approach is used for obtaining the optimal levels of different factors at a given current density. It is shown that the prediction

Table V. Analysis results at 2 A.

Methods	Test numbers	Levels				*V*stack (V)
		A	B	C	D	
Orthogonal experiment	1	1	1	1	1	18.8465
	2	1	2	2	2	20.5940
	3	1	3	3	3	21.3889
	4	2	1	2	3	19.9919
	5	2	2	3	1	21.0595
	6	2	3	1	2	19.8510
	7	3	1	3	2	20.4000
	8	3	2	1	3	19.4651
	9	3	3	2	1	21.0191
	K_1	20.2765	19.7462	19.3876	20.3084	
	K_2	20.3008	20.3729	20.5350	20.2817	
	K_3	20.2947	20.7530	20.9495	20.2820	
	R	0.0243	1.0068	1.5619	0.0267	
SVR-DSWA	Weight (%)	2.442	36.768	57.576	3.214	

Table VI. Analysis results at 12 A.

Methods	Test numbers	Levels				*V*stack (V)
		A	B	C	D	
Orthogonal experiment	1	1	1	1	1	14.7237
	2	1	2	2	2	16.7930
	3	1	3	3	3	17.7581
	4	2	1	2	3	16.3492
	5	2	2	3	1	16.9699
	6	2	3	1	2	16.0250
	7	3	1	3	2	16.5900
	8	3	2	1	3	15.7876
	9	3	3	2	1	16.9374
	K_1	16.4249	15.8876	15.5121	16.2104	
	K_2	16.4481	16.5168	16.6932	16.4694	
	K_3	16.4383	16.9069	17.1060	16.6316	
	R	0.0232	1.0193	1.5939	0.4212	
SVR-DSWA	Weight (%)	2.753	31.677	49.812	15.757	

Table VII. Analysis results at 22 A.

Methods	Test numbers	Levels				*V*stack (V)
		A	B	C	D	
Orthogonal experiment	1	1	1	1	1	9.3532
	2	1	2	2	2	14.0580
	3	1	3	3	3	15.2585
	4	2	1	2	3	13.8611
	5	2	2	3	1	13.8388
	6	2	3	1	2	11.1210
	7	3	1	3	2	13.8990
	8	3	2	1	3	11.1157
	9	3	3	2	1	13.8460
	K_1	12.8899	12.3711	10.5300	12.3460	
	K_2	12.9403	13.0042	13.9217	13.0260	
	K_3	12.9536	13.4085	14.3321	13.4117	
	R	0.0637	1.0374	3.8021	1.0657	
SVR-DSWA	Weight (%)	4.239	23.463	45.828	26.469	

accuracy of the proposed model based on the SVR algorithm is high as the RMSE is smaller than 0.0458 and R^2 is higher than 97.78%. The order of influence degree of the four factors is affected by the current levels. It is also found that the optimal operating temperature and optimal λ are different at different current density levels, while the optimal anode and cathode inlet gas pressures are not affected.

Table VIII. The influence degrees and optimal levels of different factors.

Current	Influence degree	Optimal parameters			
		A(T/K)	B(P_a/bar)	C(P_c/bar)	D(λ)
2 A	C > B > D > A	A2(348.15)	B3(3)	C3(5)	D1(14)
12 A	C > B > D > A	A2(348.15)	B3(3)	C3(5)	D3(23)
22 A	C > D > B > A	A3(353.15)	B3(3)	C3(5)	D3(23)

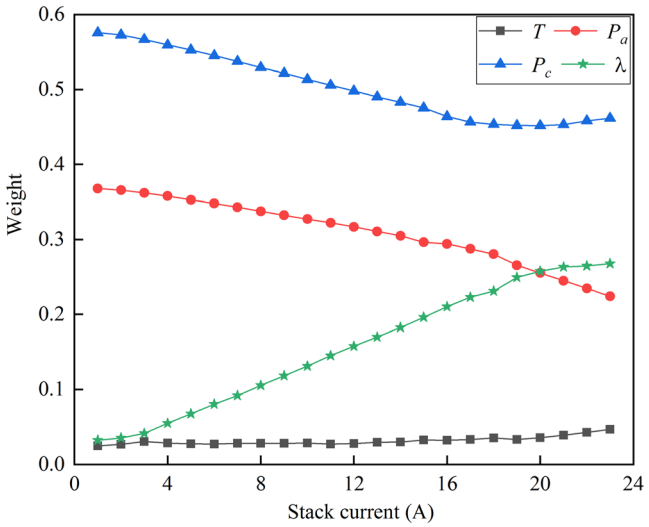

Figure 7. Weights of influence factors within the full current density range.

Furthermore, the results of the weight analysis based on the proposed SVR-DSWA algorithm are in good agreement with the single-factor simulation analysis and the orthogonal experiment. The SVR-DSWA algorithm and the standard simplex approach based on optimized SVR model are superior to the orthogonal experiment to analyze the influence degrees of input factors on the output voltage and the optimal parameter combinations within the full current density range as they take less time and are more efficient. The result can also provide a reference for the weight analysis of multiple-input influencing factors of other complex systems for future investigation.

Acknowledgments

This work was supported by the National Key Research and Development Program of China (2020YFB1506802); and Key Research and Development Project of Guangdong Province (2020B0909040004).

ORCID

Yang Yang https://orcid.org/0000-0003-1426-3912
Yang Li https://orcid.org/0000-0002-9497-3051
Chang-Jun Xie https://orcid.org/0000-0002-9626-0813

References

1. Ó. González-Espasandín, T. J. Leo, M. A. Raso, and E. Navarro, *Renew Energ*, **130**, 762 (2019).
2. O. Gröger, H. A. Gasteiger, and J. Suchsland, *J. Electrochem. Soc.*, **162**, A2605 (2015).
3. Y. Wang, K. S. Chen, J. Mishler, S. C. Cho, and X. C. Adroher, *Appl. Energ*, **88**, 981 (2011).
4. T. F. Fuller and J. Newman, *J. Electrochem. Soc.*, **140**, 1218 (1993).
5. Y. Nalbant, C. O. Colpan, and Y. Devrim, *Int. J. Hydrogen Energ*, **43**, 5939 (2018).
6. M. A. Rahman, F. Mojica, M. Sarker, and P. A. Chuang, *Electrochim. Acta*, **320**, 134601 (2019).
7. M. Abdollahzadeh, J. C. Pascoa, A. A. Ranjbar, and Q. Esmaili, *Energy*, **68**, 478 (2014).
8. P. Hong, L. Xu, J. Li, and M. Ouyang, *Energy*, **139**, 277 (2017).
9. S. Dutta, S. Shimpalee, and J. W. V. Zee, *J. Appl. Electrochem.*, **30**, 135 (2000).
10. E. E. Kahveci and I. Taymaz, *FUEL*, **217**, 51 (2018).
11. G. Zhang, J. Wu, Y. Wang, Y. Yin, and K. Jiao, *Int. J. Heat Mass Tran.*, **150**, 119294 (2020).
12. D. Hao, J. Shen, Y. Hou, Y. Zhou, and H. Wang, *International Journal of Chemical Engineering*, **2016**, 4109204 (2016).
13. M. Moore, S. Shukla, S. Voss, K. Karan, A. Weber, I. Zenyuk, and M. Secanell, *J. Electrochem. Soc.*, **168**, 44519 (2021).
14. J. M. Corrêa, F. A. Farret, L. N. Canha, and M. G. Simoes, *IEEE T Ind Electron.*, **51**, 1103 (2004).
15. R. Tirnovan, S. Giurgea, A. Miraoui, and M. Cirrincione, *J. Power Sources*, **175**, 773 (2008).
16. M. E. Youssef, K. E. Al-Nadi, and M. H. Khalil, *Int. J. Electrochem SC*, **5**, 267 (2010).
17. F. Tiss, R. Chouikh, and A. Guizani, *Int. J. Hydrogen Energ*, **38**, 8532 (2013).
18. A. L. Nascimento, I. Yahyaoui, J. F. Fardin, L. F. Encarnação, and F. Tadeo, *Int. J. Hydrogen Energ*, **45**, 30870 (2020).
19. T. Lan and K. Strunz, *Int. J. Elec. Power*, **119**, 105803 (2020).
20. Á. Hernández-Gómez, V. Ramirez, D. Guilbert, and B. Saldivar, *Renew Energ*, **163**, 1508 (2021).
21. M. M. Barzegari, S. M. Rahgoshay, L. Mohammadpour, and D. Toghraie, *Energy*, **188**, 116049 (2019).
22. S. L. Chavan and D. B. Talange, *Journal of Energy Storage*, **18**, 327 (2018).
23. F. S. Nanadegani, E. N. Lay, A. Iranzo, J. A. Salva, and B. Sunden, *Electrochim. Acta*, **348**, 136345 (2020).
24. B. Wang, G. Zhang, H. Wang, J. Xuan, and K. Jiao, *Energy and AI*, **1**, 100004 (2020).
25. R. Lin, X. Diao, T. Ma, S. Tang, L. Chen, and D. Liu, *Appl. Energ*, **254**, 113714 (2019).
26. S. Xia, R. Lin, X. Cui, and J. Shan, *Int. J. Hydrogen Energ*, **41**, 11380 (2016).
27. B. Wang, R. Lin, D. Liu, J. Xu, and B. Feng, *Int. J. Hydrogen Energ*, **44**, 13737 (2019).
28. Z. Zhong, X. Zhu, and G. Cao, *J. Power Sources*, **160**, 293 (2006).
29. C. Li, X. Zhu, G. Cao, S. Sui, and M. Hu, *J. Power Sources*, **175**, 303 (2008).
30. X. Peng, W. Wu, Y. Zhang, and W. Yang, *Journal of Energy Storage*, **13**, 409 (2017).
31. C. Wang, *Modeling and Control of Hybrid Wind/Photovoltaic/Fuel Cell Distributed Generation Systems* (ProQuest Information and Learning, Ann Arbor) (2006).
32. A. Askarzadeh and L. D. S. Coelho, *Int. J. Hydrogen Energ*, **21**, 39 (2014).
33. Z. Sun, D. Cao, Y. Ling, F. Xiang, Z. Sun, and F. Wu, *Energy*, **216**, 119056 (2021).
34. L. Zhang and N. Wang, *Int. J. Hydrogen Energ*, **38**, 219 (2013).
35. Z. J. Mo, X. J. Zhu, L. Y. Wei, and G. Y. Cao, *Int. J. Energ Res*, **30**, 585 (2006).
36. M. Derbeli, M. Farhat, O. Barambones, and L. Sbita, *Int. J. Hydrogen Energ*, **42**, 8833 (2017).